International Journal of Biological Macromolecules 132 (2019) 677–691

Contents lists available at ScienceDirect

International Journal of Biological Macromolecules

journal homepage: http://www.elsevier.com/locate/ijbiomac

Synthesis and characterization of iron oxide nanoparticles/carboxymethyl cellulose core-shell nanohybrids for killing cancer cells *in vitro*

Alice G. Leonel [a], Herman S. Mansur [a,*], Alexandra A.P. Mansur [a], Anderson Caires [a], Sandhra M. Carvalho [a], Klaus Krambrock [b], Luis Eugenio F. Outon [b], José Domingos Ardisson [c]

[a] Center of Nanoscience, Nanotechnology and Innovation - CeNano²I, Federal University of Minas Gerais - UFMG, Av. Antônio Carlos, 6627 – Belo Horizonte, MG, Brazil
[b] Department of Physics, Federal University of Minas Gerais – UFMG, Brazil
[c] Centro de Desenvolvimento da Tecnologia Nuclear – CDTN, Av. Antônio Carlos, 6627 – Belo Horizonte, MG, Brazil

ARTICLE INFO

Article history:
Received 22 January 2019
Received in revised form 22 March 2019
Accepted 2 April 2019
Available online 2 April 2019

Keywords:
Polysaccharide
Carboxymethyl cellulose
Green nanotechnology
Magnetic nanoparticle
Nanocomposite

ABSTRACT

Novel core-shell superparamagnetic nanofluids composed of magnetic iron oxide (Fe_3O_4, MION) and cobalt-doped ($Co_xFe_{3-x}O_4$, Co-MION) nanoparticles functionalized with carboxymethyl cellulose (CMC) ligands were designed and produced *via* green colloidal aqueous process. The effect of the degree of substitution (DS = 0.7 and 1.2) and molecular mass (M_w) of CMC and cobalt doping concentration on the physicochemical and magnetic properties of these nanoconjugates were comprehensively investigated using Fourier-transform infrared spectroscopy (FTIR), X-ray diffraction, transmission electron microscopy (TEM) with selected area electron diffraction, X-ray fluorescence, dynamic light scattering (DLS), zeta potential (ZP) analysis, vibrating sample magnetometry (VSM) and electron paramagnetic resonance spectroscopy (EPR). The results demonstrated the effect of concentration of carboxylate groups and M_w of CMC on the hydrodynamic dimension, zeta potential, and generated heat by magnetic hyperthermia of MION nanoconjugates. Co-doping of MION showed significant alteration of the electrostatic balance of charges of the nanoconjugates interpreted as effect of surface interactions. Moreover, the VSM and EPR results proved the superparamagnetic properties of these nanocolloids, which were affected by the presence of CMC and Co-doping of iron oxide nanoparticles. These magnetic nanohybrids behaved as *nanoheaters* for killing brain cancer cells *in vitro* with prospective future applications in oncology and nanomedicine.

1. Introduction

Despite the unquestionable scientific and technological developments in recent decades, cancer remains one of the deadliest diseases worldwide. Unfortunately, conventional cancer therapies such as chemotherapy and radiotherapy predominantly focused on cell killing treatments without achieving high specificity, which often resulted in systemic toxicity and harsh side-effects. Therefore, innovative alternatives of novel tumor-targeted therapies are urgently required, which can effectively and specifically reach cancer cells while minimizing the toxicity towards healthy cells and tissues [1–6]. Emerging nanotechnologies offer promising opportunities for drastically altering this scenario based on a large arsenal of novel nanomaterials, which have been developed in the past decades. They can contribute with diversified options for fighting cancer, from the early diagnosis through functional nanoprobes associated with tumor targeting therapies using nanocarriers for smart delivery of drugs [2–6]. Hence, multifunctional nanomaterials have drawn significant attention as promising candidates for tumor-targeting applications [7–9]. In particular, magnetic iron oxide nanoparticles have been intensively investigated because of the unique property to respond well to magnetic control. Their properties can be tuned by morphological features (*e.g.*, size, shape, structure) and chemical composition (*e.g.*, ion doping, Co, Ni, *etc.*) directing for several advanced applications, including information storage, protein purification, biological separation, drug delivery and environmental remediation using iron oxide nanoparticles as sorbents and photocatalysts [7–13]. In addition, magnetic iron oxide nanoparticles possess a significant set of features, including biocompatibility, physicochemical stability and relative low toxicity. Therefore, they have been researched for a broad range of biomedical applications such as in cellular labeling, drug nanocarrier, gene delivery, MRI biomedicine, magnetic hyperthermia, *etc.* [7–9]. However, in order to further achieve the highest possible selectivity at targeting the tumor site, a new class of hybrid nanomaterials composed of inorganic-organic architectures has

* Corresponding author at: Federal University of Minas Gerais, Av. Antônio Carlos, 6627 – Escola de Engenharia, Bloco 2 – Sala 2233, 31.270-901, Belo Horizonte, MG, Brazil.
E-mail address: hmansur@demet.ufmg.br (H.S. Mansur).

https://doi.org/10.1016/j.ijbiomac.2019.04.006
0141-8130/

awakened widespread interest as *smart* multifunctional nanoplatforms. They are capable of simultaneously performing diagnosis, targeting and therapy of cancer, which is commonly referred to as nanotheranostics.

In this sense, to develop magnetic nanoconjugates for applications in cancer nanomedicine, the selection of the appropriate biological molecule as the active organic coating on the surface of the inorganic nanoparticle is of pivotal importance to effectively perform the designed functions [7–8]. These hybrid nanoparticulate systems have to combine the magnetic properties of the inorganic nanoparticles, with the morphological features (size, size distribution, shape, *etc*.), the physicochemical characteristics of surface (*e.g*., surface charges, chemical groups, chemical stability in aqueous medium, *etc*.), and the biological compatibility, which will determine their outcome towards biomedical applications [14–16].

Among the several alternatives of molecules for biological and biomedical applications, natural polymers such as polysaccharides (*e.g*., cellulose and derivatives) have been widely used mainly owing to their inherent nontoxicity and abundance. Carboxymethyl cellulose (CMC) is a very important cellulose derivative with carboxylate and hydroxyl functional groups, with a unique set of characteristics such as natural, green, hydrophilic, nontoxic, biocompatible and biodegradable, inexpensive, and chemically stable. Moreover, CMC is FDA approved for a broad range of purposes, including nutrition (*e.g*., thickening and emulsifying agent in foods), biomedical and pharmaceutical applications (*e.g*., controlled drug delivery systems, gene delivery nanocarriers) [4,7,17,18].

The concept of multifunctional nanomaterials was investigated in an elegant paper reported by S. Balasubramanian and *co*-workers [7] where they reported a two-step process for the synthesis of magnetic iron oxide nanoparticles in water medium with subsequent dispersion in CMC polymer solution. It was demonstrated the feasibility of these nanoconjugates to be guided through magnetic fields for biomedical applications such as drug delivery systems and oncological therapy by magnetic hyperthermia of cancer cells. Essentially, the cancer therapy based on magnetic hyperthermia increases locally the temperature of tumors by 5–6 °C (typically reaching 41–46 °C) using magnetic nanocolloids dispersed in aqueous media when they are subjected to an external alternating magnetic field (AMF). This approach selectively heats up the cancer cells which internalized the target magnetic nanoparticles, to prevent damage to adjacent healthy tissues of the body by acting as localized *"nanoheaters"* [8,9,16,19,20].

Surprisingly, despite the increasing interest on this fascinating field of research with some studies published on polysaccharide-magnetic nanoparticles [7–9,17,21,22], no report was found in the consulted literature investigating the direct synthesis of magnetic iron oxide nanoparticles using CMC polymers with distinct degree of substitution (*i.e*., DS, concentration of carboxylic groups) and molecule mass (M_w) as biocompatible ligands for tuning the physicochemical and magnetic properties of colloidal nanohybrids. In addition, it was observed the lack of reports exploring the comprehensive characterization of the nanoconjugates and the correlation of properties with the magnetic hyperthermia behavior under AMF for killing brain cancer cells *in vitro*.

Thus, in this study, we demonstrated for the first time that magnetic iron oxide nanoparticles (MIONs) can be synthesized by a single-step one-pot green process in aqueous medium using natural cellulose derivative, CMC, simultaneously acting as stabilizing ligand and functional biocompatible organic coating. Moreover, the molecular mass and the degree of substitution of CMC affected the surface properties and balance of charges during the formation of iron oxide nanocolloidal dispersions. In addition, the effects on the properties by doping the iron oxide nanoparticles with cobalt ions during the synthesis were investigated and compared to undoped nanofluids. In summary, these systems were designed, produced and behaved actively as superparamagnetic nanocolloids under alternating magnetic field causing an increase of temperature by thermal heating (*i.e*., referred to as nanoheaters). The magnetic behavior was affected by the processing parameters, including cobalt-doping the iron oxide nanoparticles, altering the concentration of carboxylic groups (DS) and M_w of the CMC ligand layer.

2. Materials and methods

2.1. Materials and cell cultures

Sodium carboxymethyl cellulose (CMC) with two degree of substitution, DS = 0.7 (CMC_07_90, Product Number: 419273, average molar mass M_w = 90 kDa, viscosity 180 cps, 4% in H_2O at 25 °C; and CMC_07_250, Product Number: 419311, M_w = 250 kDa and, viscosity 735 cps, 2% in H_2O at 25 °C) and DS = 1.2 (CMC_12_250, Product Number: 41281, M_w = 250 kDa and, viscosity 660 cps, 2% in H_2O at 25 °C), ferric chloride hexahydrate ($FeCl_3$•$6H_2O$, 97%), ferrous sulfate heptahydrate ($FeSO_4.7H_2O$, 99%), cobalt (II) acetate tetrahydrate ($Co(C_2H_3O_2)_2$•$4H_2O$, 98%) and ammonium hydroxide (NH_4OH, 28–30% NH_3 in H_2O) were supplied by Sigma-Aldrich (USA). The aforementioned chemicals were used without further purification. Deionized water (DI water, Millipore Simplicity™) with resistivity of 18 MΩ.cm was used to prepare all the solutions, and the procedures were performed at room temperature (RT, 25 ± 2 °C), unless specified otherwise.

Human embryonic kidney (HEK 293 T, American Type Culture Collection - ATCC® CRL 1573™) cells were provided by Federal University of Minas Gerais/UFMG. Human glioma (U87, ATCC® HTB-14) cells were purchased from Brazilian Cell Repository (Banco de Células do Rio de Janeiro: BCRJ, Brazil; cell line authentication molecular technique, *Short Tandem Repeat* (*STR*) *DNA*; quality assurance based on the international standard NBR ISO/IEC 17025:2005).

2.2. Synthesis of magnetic iron oxide nanoconjugates (MION-CMC)

Magnetic iron oxide nanoparticles (MIONs) were prepared similar to the method previously reported [7], which was based on the coprecipitation of Fe(II) and Fe(III) oxide nanoparticles in water medium in the presence of NH_4OH at 80 ± 2 °C under nitrogen atmosphere. However, in this study, the innovation relied on the synthesis performed using a single-step one-pot process, where the iron oxide nanoparticles were formed and stabilized directly by CMC as colloidal aqueous solution without requiring the subsequent dispersion of the nanoparticles in polymer medium. The process of synthesis of MIONs is schematically illustrated in Fig. 1. In brief, 0.02 M of $FeSO_4$ and 0.04 M of $FeCl_3$ were dissolved in the CMC solution (1.0% w/v, 200 mL) and heated to 40 ± 2 °C under vigorous stirring. Then, the mixture was heated up to 80 ± 2 °C under nitrogen atmosphere and 12 mL of NH_4OH solution (25.0% v/v) was added to the reaction flask and homogenized under moderate stirring for 20 min. Then the solution was cooled down to room temperature and dialyzed for 24 h using cellulose membrane (M_w cut-off of 12 kDa) under moderate stirring at room RT. After purification, the colloidal solution was stored at 6 ± 2 °C for further use. For the synthesis of cobalt-doped nanoparticles (Co-MIONs) a similar procedure was performed except for the amount of Fe^{2+} precursor used. In that case, Fe^{2+} species were partially replaced by 3.0% or 5.0% (mol/mol) of Co^{2+} species. Table 1 summarizes the identification and composition of the nanoconjugates (nanoparticles with CMC ligand). As the reference, uncoated magnetite nanoparticles were also prepared using a similar protocol without the addition of CMC in the medium (*i.e*., without capping ligand).

2.3. Physicochemical, morphological and magnetic characterization of CMC and iron oxide nanoconjugates

Physicochemical characterization of CMC was performed as previously reported by our group [23] using Fourier-transform infrared spectroscopy (FTIR) and ^1H nuclear resonance spectroscopy (^1H NMR) analyses (detailed protocol in *Supplementary Material*). Considering

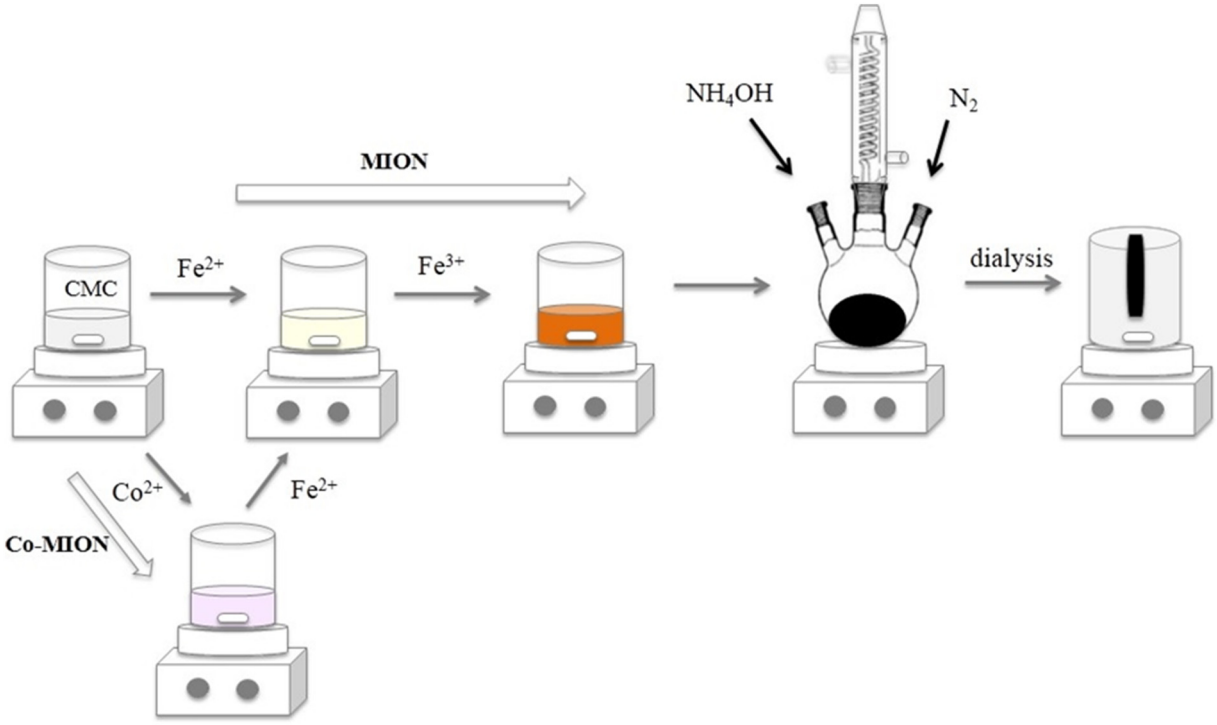

Fig. 1. Schematic representation of the synthesis of iron oxide nanoparticles (MIONs) and Co-doped MION (Co-MIONs) stabilized by CMC.

that the results of NMR and FTIR are complemented by the M_w and DS analyses provided by the supplier, a more in-depth analysis was not required and it is beyond the scope of this study.

The iron oxide nanoconjugates (MION-CMC and Co-MION-CMC) were extensively characterized in order to access their major properties essential for the designed system. X-ray diffraction (XRD) patterns were recorded using PANalytical (Almelo, Netherlands) Empyrean diffractometer (Cu-Kα radiation with $\lambda = 1.54056$ Å). Measurements were performed in the 2 theta range from 3.03 to 89.97° with steps of 0.06°. For the sample preparation, the nanoparticle suspensions were placed onto glass slides and oven-dried at 40 ± 1 °C for 1 h.

Wavelength dispersive X-ray fluorescence spectrometry (WD-XRF) measurements were performed on a Supermini200 spectrometer (Rigaku Corporation, Tokyo, Japan) and cobalt concentration was determined from the Co kα line intensity. The samples were prepared by adding 2 mL of the colloidal solutions into plastic dishes (molds) and drying at 40 ± 1 °C for 24 h for the formation of the films.

Transmission electron microscopy (TEM) images, selected-area electron diffraction (SAED) patterns, and energy-dispersive X-ray (EDX) spectra were obtained using a Tecnai G2-20 (FEI Company, Inc., Hillsboro, USA) microscope at an accelerating voltage of 200 kV. Samples were prepared by placing droplets of diluted suspensions of iron oxide nanoconjugates onto the carbon-coated copper grids and allowing them to dry at room temperature. The average nanoparticle size and size-distribution data were obtained based on the TEM images by measuring at least 100 randomly selected nanoparticles using image-processing program (DigitalMicrograph®).

FTIR spectra were obtained by direct transmission method from films (Thermo Fischer, Nicolet 6700, Massachusetts, USA) over the range from 400 to 4000 cm^{-1} using 64 scans and the resolution of 2 cm^{-1}.

Dynamic light scattering (DLS) and zeta potential (ZP) analysis were performed using a ZetaPlus instrument (Brookhaven Instruments Corporation, New York, USA) with a laser light wavelength of 660 nm (35-mW red diode laser). For both analyses, the colloidal suspensions were diluted in previously filtered deionized water (0.45 μm aqueous syringe filter – Millex LCR 25 mm, Millipore). The measurements were conducted at 25 ± 2 °C and the light scattering was detected at 90°. At least three measurements were obtained for each nanoconjugate system and the average and standard deviation (SD) were calculated.

Electron paramagnetic resonance spectroscopy analysis (EPR) was carried out on commercial X-band EPR spectrometer (Magnettech - Germany, model Miniscope MS400) coupled to helium flux cryosystem (Oxford - England, model ESR 900). The standard parameters applied for all measurements were: center field 350 mT, sweep range 500 mT, 30 dB microwave power (~100 μW), microwave frequency about 9.44 GHz, 100 kHz field modulation. All samples were measured in powder form after drying inside borosilicate tubes at 120 °C (Wilmad Labglass - USA).

Magnetization curves as a function of temperature were measured with a vibrational sample magnetometer (VSM) from Lake Shore, USA, model 7404. For the measurements, the following protocol was used: (i) cooling the samples in zero-field from 300 K to 77 K; (ii) after reaching 77 K, a field of 70 Oe was applied and the magnetic moment measured as a function of temperature from 77 K to 300 K (zero-field cooling, ZFC); and (iii) after reaching 300 K, the magnetic moment of samples was measured again from 300 K to 77 K with the applied field (field cooling, FC). Magnetic hysteresis curves M(H) were measured in the field range − 10.000 Oe < H < 10.000 Oe at 77 K and 300 K from which coercivity field and saturation magnetization were determined.

Table 1
Experimental conditions for the synthesis of MION and Co-MION nanoconjugates.

Sample	Degree of substitution (DS) of CMC	M_w of CMC (kDa)	Cobalt content (% mol/mol)
MION-CMC_07_90	0.7	90	0
MION-CMC _07_250	0.7	250	0
MION-CMC_12_250	1.2	250	0
Co3-MION-CMC_07_90	0.7	90	3.0
Co5-MION-CMC_07_90	0.7	90	5.0

2.4. Biological characterization of MION and Co-MION

2.4.1. Cell viability in vitro – Mitochondrial activity (MTT) assay

MTT (3-(4,5-dimethylthiazol-2yl-) 2,5-diphenyl tetrazolium bromide) experiments were performed to preliminarily accessing biocompatibility of iron oxide nanoparticles in different concentrations after incubation with HEK 293 T (normal) and U87 (cancer) cells for 24 h (detailed protocol in *Supplementary Material*).

2.5. Magnetic hyperthermia of nanocolloids

2.5.1. Magnetic hyperthermia test in vitro acellular

Magnetic hyperthermia analyses were performed using a Magnetherm™ instrument (Staffordshire, United Kingdom, solenoid diameter D = 50 mm, number of turns $N = 17$). The samples were exposed to alternating magnetic field (AMF) with amplitude of 19.9 kA/m and frequency of 112.6 kHz for 30 min.

2.5.2. Magnetic hyperthermia in vitro with brain cancer cells

The magnetic hyperthermia (MT) experiments were performed according to the protocol detailed in the *Supplementary Material*. Briefly, the MION-CMC sample (at concentration = 15 μg/mL) was incubated with brain cancer cells for 3 h for allowing the cellular uptake of the nanoconjugates. Next, these incubated cancer cells as well as the reference samples (*i.e.*, positive and negative controls) were exposed to the AMF with amplitude of 19.9 kA/m and frequency of 112.6 kHz for 60 min (Magnetherm™, Staffordshire, United Kingdom). After the exposure, the cells were washed, trypsinized, counted (number of dead and live cells) and the percentage of cell viability was expressed relative to the live cells. Normal cells were not assayed by MT because it is ideally focused on killing cancer cells by the heat generated by AMF, which requires specific targeting tumor cells not present in this study.

3. Results and discussion

3.1. Characterization of CMC polymer

Initial spectroscopic characterization of the different CMC samples (DS = 0.7 and 1.2; M_w = 90 and 250 kDa) was performed by FTIR (Fig. 1Ss) and ^{1}H NMR (Fig. 2S) analyses and the results are presented in *Supplementary Material*. As expected, the FTIR spectra showed the presence of the most relevant functional groups of CMC polymer (hydroxyls, carboxylic and/or carboxylates). In addition, the peaks associated with the carboxylates were relatively more pronounced for CMC with DS = 1.2 compared to DS = 0.7 due to the higher concentration of these groups. In the ^{1}H NMR spectra, resonance signals associated with unsubstituted and substituted hydroxyl groups were detected. The integration of the unsubstituted protons signals for CMC polymers indicated the decrease in the relative intensity of OH groups for CMC of DS = 1.2 accounted for the higher content of COO^- groups compared to DS = 0.7.

3.2. Physicochemical and morphological characterization of MION and co-MION

The XRD analysis of the iron oxide nanoconjugates (Fig. 2A (b) and (c)) confirmed the formation of an inverse spinel structure of magnetite (JCPDS 89-0691) supported by the peaks observed at 30.1°, 35.5°, 43.1°, 57.0°, and 62.6° corresponding to the orientations along (220), (311), (400), (511), and (440) planes, respectively. The broad band at 21.8°, observed in both samples, is characteristic of the CMC (Fig. 2A (a)). Additionally, it was not detected the formation of other iron oxides (*e.g.*, γ-Fe_2O_3, JCPDS 25-1402; and α-Fe_2O_3, JCPDS 87-1166) or iron oxide hydroxides (JCPDS 81-0463 and JCPDS 76-2301). Thus, the XRD results (Fig. 2A and Fig. 3S, *Supplementary Material*) demonstrated that only Fe_3O_4 (magnetite) nanoparticles were produced using the one-pot synthesis in aqueous media for all conditions of DS or M_w values of CMC ligands. Moreover, XRD patterns were also employed for assessing the effect of doping the iron oxides with cobalt ($Co_xFe_{3-x}O_4$, x = 0, 0.03 and 0.05) based on the nanocrystallite size (τ) using the Scherrer's equation (full width at half maximum, FWHM) [24]. The results in Fig. 2B indicated the average size of the nanocrystallites of iron oxides ranging from 6 to 10 nm. The doping of Fe_3O_4 nanoparticles with Co^{2+} during the synthesis reduced the average size of nanocrystal by approximately 30% (*i.e.*, from 10 nm to 7 nm), which was assigned to the partial replacement of Fe^{2+} (ionic radius = 0.77 Å) with Co^{2+} (ionic radius = 0.74 Å). This difference of ionic radius may have caused the "shrinkage" of unit cell according to the literature [24,25]. These results of Scherrer's equation can also be used as a preliminary calculation of the dimension of the nanoparticles, which indicated the reduction of the average size by incorporating Co^{2+} in the iron oxide structure (*i.e.*, from Fe_3O_4 to $Co_xFe_{3-x}O_4$).

In Fig. 2C is presented the WD-XRF spectra of the Fe_3O_4 (a) and Co-doped Fe_3O_4 nanoparticles (b), where the Co5-MION-CMC_07_90 sample showed two peaks located at 2 theta = 52.8° and 47.5° corresponding to the Co Kα and Co Kβ transitions, respectively [26]. The quantitative chemical analysis of Co by WD-XRF revealed the concentration of 1.5% mol (in relation to total iron content, Fe^{2+} and Fe^{3+}). This result is in good agreement with the estimated theoretical value of 1.7% (or equivalent to 5% mol in relation of Fe^{2+}) used in the synthesis of the nanocolloids. Therefore, these results evidenced that Co^{2+} species were successfully incorporated into the structure of magnetite nanoparticles by the partial replacement of Fe^{2+} ions in the nanocrystals.

TEM analysis was performed to access the morphological features of the iron oxide nanoparticles capped by CMC ligand. It was observed in TEM images (Fig. 3 and Fig. 4S–7S, *Supplementary Material*) that magnetite and Co-doped magnetite nanoparticles were produced with spherical morphology (Fig. 3A) and with average size ranging from 7 to 10 nm (Fig. 3B). Therefore, no significant trend was observed considering the DS and M_w parameters of the biopolymer CMC or the cobalt concentration on modifying the average size of the colloidal iron oxide nanoparticles (within the statistical variation). These results were interpreted as the combination of several effects, including the concentration of reagents and the characteristics of the CMC (carboxylic functional groups, molar mass) on the overall nucleation and growth processes of iron oxide nanoparticles, causing the formation of highly stable nanocolloids in aqueous media minimizing the influence of these parameters on the final size of the nanoparticles.

The crystallinity of MION and Co-MION nanocolloids was also investigated by high resolution transmission electron microscopy imaging (HRTEM) associated with selected area electron diffraction (SAED) analysis. The presence of interference fringes with average distances of 2.5 Å (Fig. 3C) was associated with the interatomic distances of (311) plane of spinel ferrite, which confirmed the crystallinity of the iron oxide nanoparticles. The SAED patterns (Fig. 3D) consisted of concentric diffraction rings characteristic of iron oxide nanoparticles. They were indexed as (220), (311), (400), (511), and (440) planes of cubic spinel structure of ferrites, as discussed previously with XRD results, with respective d-spacing (d ± 0.05 Å) of 3.00, 2.60, 2.20, 1.60, 1.50 Å for Co5-MION-CMC_07_90 sample [25].

The FTIR spectra of CMC (a), MION-CMC (b) and Co-MION-CMC (c) are shown in Fig. 4A. It was observed in the CMC spectrum the presence of a broad band at 3400–3200 cm^{-1} assigned to νO—H vibrations and the bands related to asymmetric (1652 and 1590 cm^{-1}) and symmetric (1420 and 1320 cm^{-1}) stretches of carboxylate groups of CMC. Additionally, it was detected the vibrations of C—O associated with secondary alcohols (νC2-OH; 1113 cm^{-1} and νC3-OH; 1060 cm^{-1}) and the vibrational band at 890 cm^{-1} associated with the β1–4 glycoside bonds. Moreover, bands assigned to δO—H vibrations were observed in the range from 710 to 600 cm^{-1}. However, the fact that these bands are located in regions overlapping with other bands limit their application as an accurate structural identification tool [7,27]. The comparison of FTIR

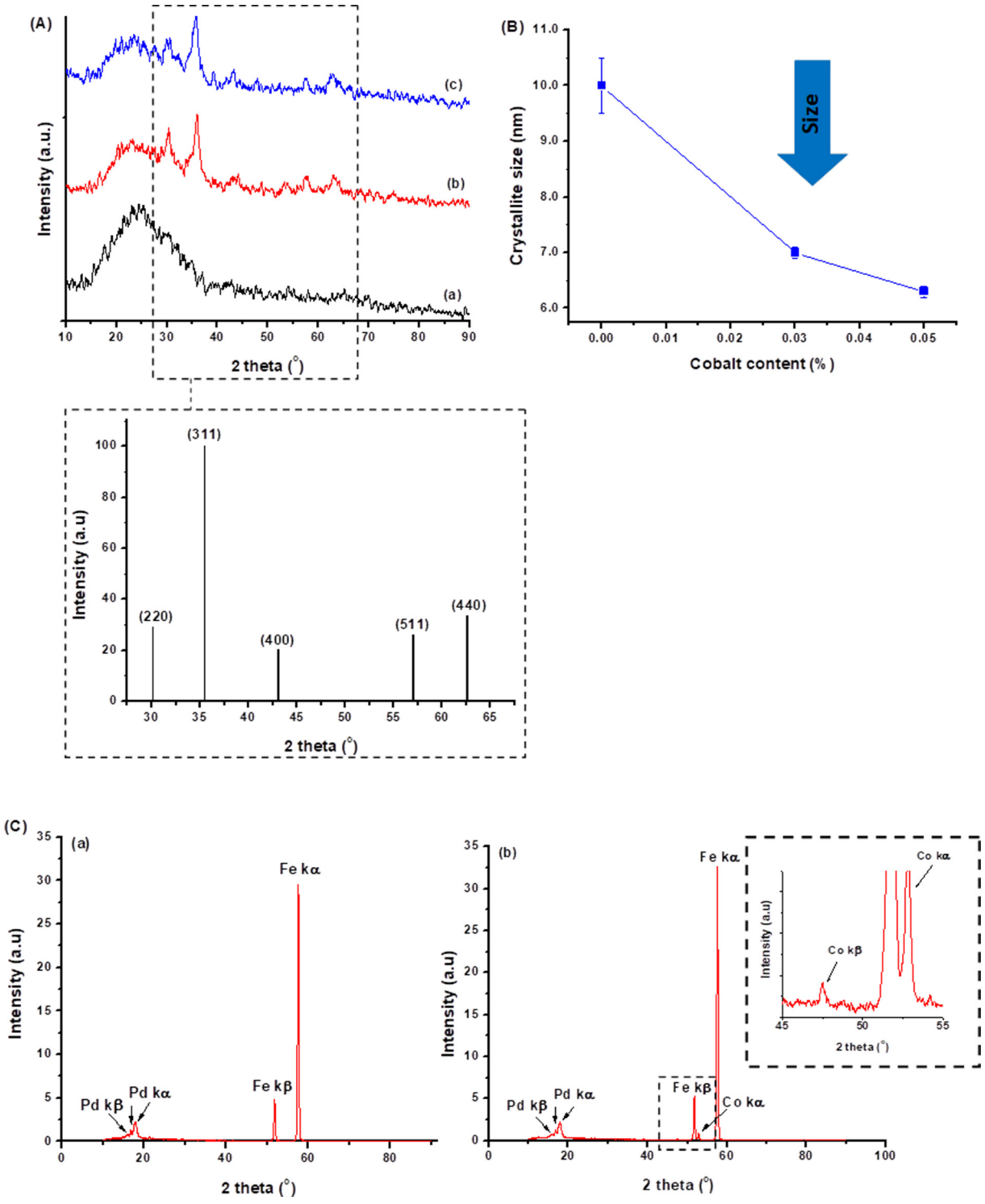

Fig. 2. (A) XRD patterns of (a) CMC_07_90, (b) MION-CMC_07_90 and (c) Co5-MION-CMC_07_90 samples (top) compared with the reference pattern of Fe_3O_4 (Bottom, JCPDS 89–0691). (B) Effect of the cobalt content in the iron oxides on average size of the nanocrystallite. (C) WD-XRF spectra of (a) MION-CMC_07_90 and (b) Co5-MION-CMC_07_90 nanocolloids.

spectra of CMC (Fig. 4A (a)) with MION-CMC and Co-MION-CMC nanocolloids (Fig. 4A (b) and (c)) indicated the appearance of bands centered at 590 cm^{-1} assigned to νFe-O vibrations. The characteristic Fe—O vibration of bulk magnetite occurs at 570 cm^{-1}, however, according to the literature [7,28], when the particles were reduced to nanoscale dimensions, the absorption band of Fe—O bond shifts to higher wavenumbers (at 640 and 589 cm^{-1}). As expected, the same bands were also observed for the other samples of iron oxide nanoconjugates, MION-CMC_07_250, MION-CMC_12_250 and Co3-MION-CMC_07_90 (Fig. 8S, *Supplementary Material*). In order to analyze the doping of iron oxide nanoparticles with Co, the region of the FTIR spectra from 950 to 550 cm^{-1} was enlarged and presented in Fig. 4B. However, considering that the stretching vibration of octahedral group Co—O (region II) occurs in the same region of the stretching vibration of Fe—O (region III), it was necessary to perform the deconvolution of the spectra ((b) MION-CMC_07_90 and (c) Co5-MION-CMC_07_90) to verify the influence of cobalt doping on magnetite nanoparticles. In this sense, semi-quantitative analysis was performed based on the ratio of the

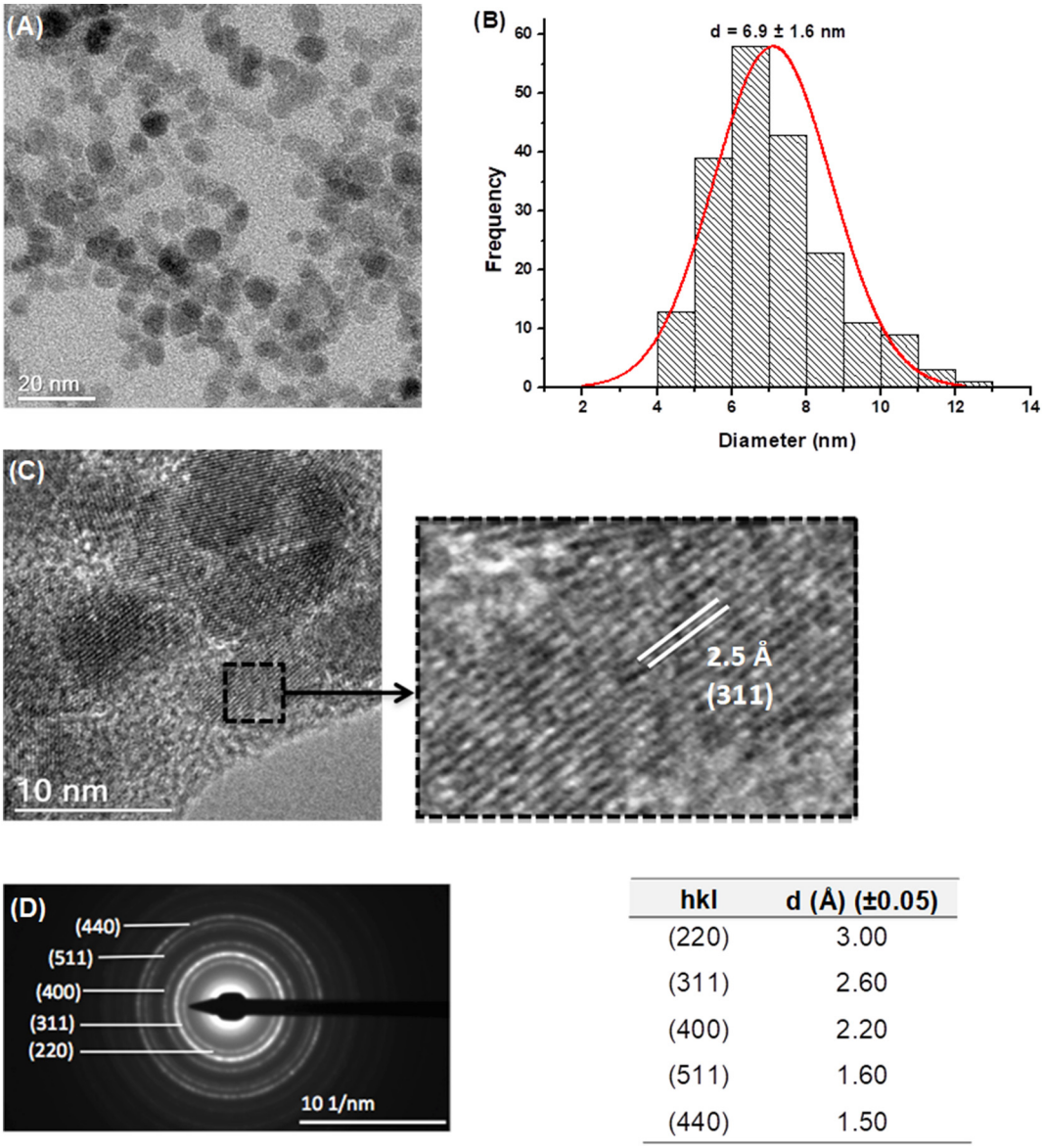

hkl	d (Å) (±0.05)
(220)	3.00
(311)	2.60
(400)	2.20
(511)	1.60
(440)	1.50

Fig. 3. Characterization of Co5-MION-CMC_07_90 nanoparticles: (A) TEM image; (B) Histogram of size distribution; (C) HRTEM image with interplanar distance between lattice fringes (detail); (D) SAED pattern (left) with d-spacing of lattice planes in the nanocrystal (right).

areas of Co—O (region II, Fig. 4B) and Fe—O (region III, region II, Fig. 4B) bands, relative to the β1-4 (region I, Fig. 4B) band, used as reference. It was verified (Fig. 4C) a relative reduction of the band assigned to Fe—O vibrations (~590 cm^{-1}) [7,24,28] and an increase in the band assigned to Co—O vibrations (~600–615 cm^{-1}) [29,30], as the result of the cobalt doping of the magnetite nanoparticles.

According to the literature [27,31], the difference of wavenumber between the asymmetric and symmetric vibrations of the COO^- groups ($\Delta\nu$, Table 1S, *Supplementary Material*) can be used to indicate the mode of the carboxylate binding to metal ions on forming coordination complexes. Here, the $\Delta\nu$ values suggested two different types of coordination, monodentate and bidentate bridging as it illustrated in Fig. 4D. Due to the high surface to volume ratio of very small nanoparticles (*i.e.*, <20 nm), it is expected that the under-coordinated metallic ions at their surface have played a pivotal role for the formation of complexes with the CMC ligand *via* functional groups (*e.g.*, COOH/COO^-). Based on the results, these interactions at the nanointerfaces (MION-CMC) were not significantly altered by the characteristics of CMC (DS and M_w) or cobalt content (Fig. 8S and Table 1S, *Supplementary Material*).

To further characterize the colloidal behavior of these nanoparticles in aqueous system, DLS analysis was performed. The hydrodynamic diameter (d_h) of Fe_3O_4 nanoparticles stabilized by different CMC polymers ranged from 63 to 125 nm (Fig. 5A). These results evidenced the influence of DS and M_w on the overall interactions occurring at the nanoparticle-polymer interfaces and the balance of charges among all molecules in the medium. The MION-CMC_07_90 sample showed the lowest average d_h, which was interpreted by considering that d_h in nanocolloids corresponds to the sum of the inorganic core and the polymeric shell [32], the smaller M_w of CMC (90 kDa) should contribute to decrease the d_h. Moreover, comparing MION-CMC_07_250 and MION-CMC_12_250 samples (M_w = 250 kDa), it was observed that MION-CMC_12_250 showed higher d_h. This behavior was assigned to the fact that the higher concentration of COO^- groups (DS = 1.2 > 0.7) may have caused the repulsion between adjacent polymer chains and higher interaction with water molecules, which increased the total volume of solvation and the d_h [1]. In Fig. 5B is plotted the percentage of relative increase of the d_h values of MION-CMC_07_250 and MION-CMC_12_250 compared with MION-CMC_07_90 sample. These results

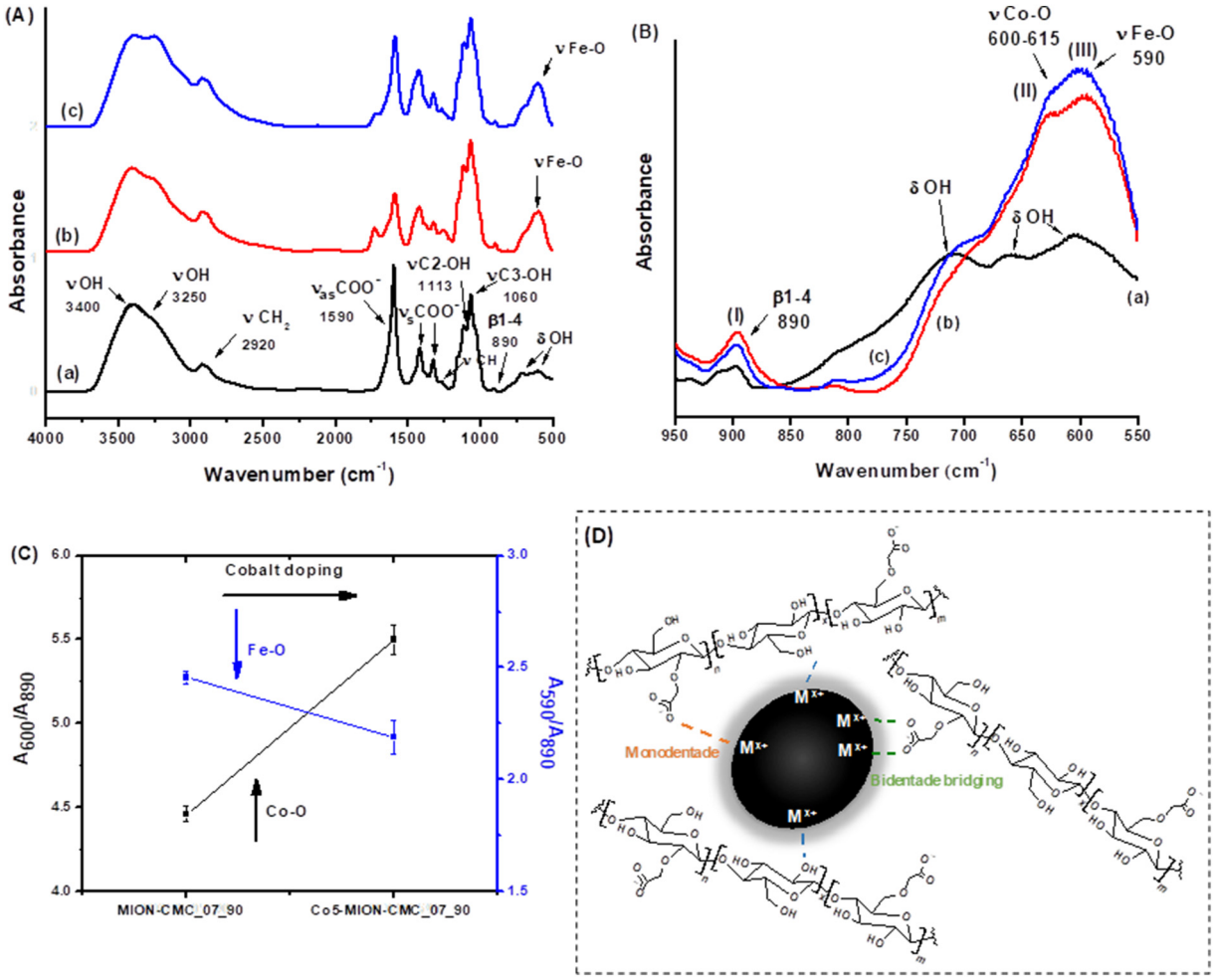

Fig. 4. (A) FTIR spectra of nanoconjugates: (a) CMC_07_90, (b) MION-CMC_07_90 and (c) Co5-MION-CMC_07_90 samples. (B) Detail of the FTIR spectra region associated with the range of β1-4, Fe—O and Co—O vibrations. (C) Evolution of Fe—O and Co—O bands due to cobalt doping. (D) Schematic representation of nanoparticles/CMC interactions (not to scale).

demonstrated that the M_w of cellulose derivative (CMC) and the concentration of carboxylate functional groups (DS) were responsible for increasing d_h by 55% and 98%, respectively. It should be highlighted that, during the synthesis of nanoparticles *via* an aqueous colloidal chemistry, there are several parameters for altering and controlling their sizes and physicochemical properties, including the selection of chemical precursors, ligands, concentration, and others [32].

These results are very relevant bearing in mind the potential biomedical applications of the nanoconjugates, as the hydrodynamic size is one of the key aspects on the interactions of nanomaterials with living cells and biological systems.

The ZP values of approximately ~ −70 mV were similar for the iron oxide nanoparticles (MIONs) indicating they were effectively stabilized by COO^- functional groups of CMC mostly by electrostatic repulsion mechanism (*i.e.*, ZP ≪ −30 mV), although steric hindrance cannot be ruled out [27]. For comparison, without the presence of the CMC macromolecule as ligand, the uncoated Fe_3O_4 nanoparticles presented ZP and d_h values of -16 ± 7 mV and 31 ± 2 nm, respectively. It was clearly observed the reduction of ZP without the negative carboxylate groups and the decrease of d_h value due to the absence of the CMC polymer, *i.e.*, the organic shell surrounding the iron oxide nanoparticles.

The comparison of DLS analysis of MION_07_90 and Co-MION samples (Fig. 6A) evidenced a significant difference due to the cobalt-doped iron oxide nanoparticles despite they were capped with the same CMC polymer. The higher d_h value of Co-MION (Fig. 6B) was suggested to be caused by the formation of more stable and larger Co(II) carboxylate complexes at the nanointerface (nanoparticle-polymer) as depicted in Fig. 6C. This event improved the degree of freedom of Co^{2+} species at the coordination structure permitting higher interactions with water molecules, which increased the volume of solvation and consequently, the value of d_h, as supported by the literature [33,34].

Similarly to MION nanoconjugates, the ZP values of Co-MION-CMC systems indicated that they were also chemically stabilized as nanocolloids by COO^- groups of CMC mostly due to electrostatic repulsion [27]. However, the Co5-MION-CMC_07_90 nanoparticles presented a relative decrease of ~20% in the negative surface charges (~−58 mV) compared to analogous Fe_3O_4 nanoparticles (~−69 mV). This trend was attributed to the relative higher value of d_h of Co-doped nanocolloids, which facilitated the conformation of carboxylate groups and the polymer chain of CMC in water medium for minimizing the electrostatic repulsions (*i.e.*, free energy), affecting the overall balance charges.

3.3. Magnetic characterization of MION and Co-MION

The EPR spectra as a function of temperature (T) of (A) MION-CMC_07_90, (B) Co5-MION-CMC_07_90 and (C) uncoated magnetite nanoparticles, are presented in Fig. 7. These EPR spectra are characteristic for superparamagnetic nanoparticles in highly concentrated systems. The resonance lines are shifted to lower fields, losing intensity, line shapes are broadened and becoming more isotropic for decreasing temperatures [35–37]. While the resonance lines of coated MION-CMC_07_90 showed similar behavior as a function of temperature compared with the uncoated magnetite nanoparticles, the resonance lines of

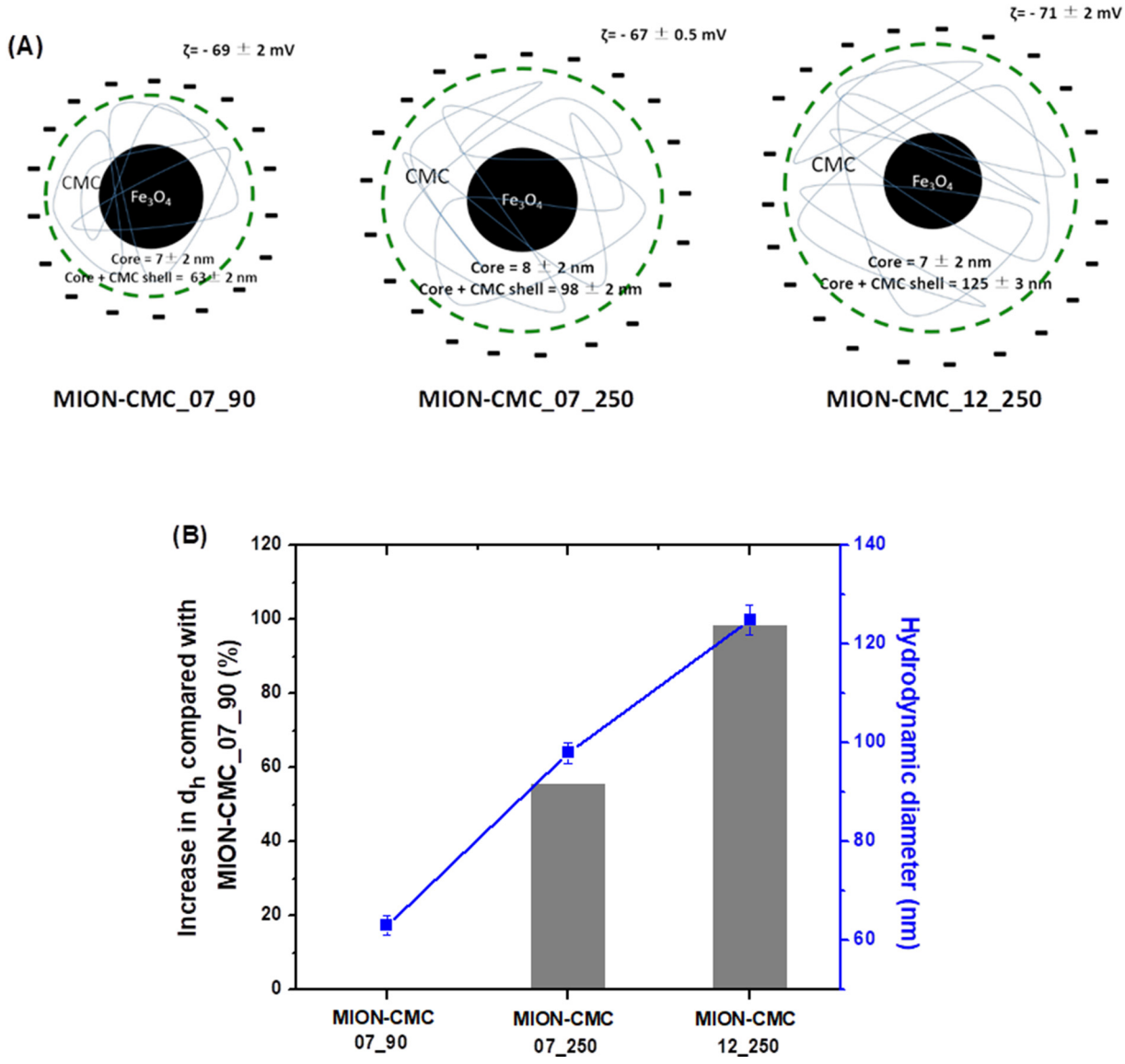

Fig. 5. (A) Schematic representation of core-shell nanostructures of MION-CMC_07_90, MION-CMC_07_250 and MION-CMC_12_250 (pH = 7.0 ± 0.5). (B) Percentage of relative increase on d_h of MION-CMC_07_250 and MION-CMC_12_250 samples compared with MION-CMC_07_90.

the Co5-MION-CMC_07_90 showed much stronger anisotropic temperature dependence. In general, nanoparticles consisting of Co-spinels present higher magnetocrystalline anisotropy due to the spin-orbit contributions resulting in magnetically harder materials when compared with Fe-spinels, which are magnetically softer [38]. However, it is still unexpected that the relative low Co-doping of 5% in Fe-spinels resulted in such significant change in the resonance lines.

Thus, in order to confirm the superparamagnetic behavior and the important difference observed in the resonance spectra between MION-CMC and Co-MION-CMC conjugates, magnetization curves of all samples were measured and are shown in Fig. 8 for both zero-field cooling (ZFC) and field cooling (FC) in a field of 70 Oe. In addition, Fig. 9 shows the hysteresis curves for the samples under evaluation measured at 77 K and 300 K as a function of the magnetic field (−10,000 Oe < H < 10,000 Oe).

In accordance with the EPR measurements, the magnetization measurements show clearly that all three samples are superparamagnetic at room temperature, *i.e.*, no sample shows hysteresis at 300 K (Fig. 9). Superparamagnetic nanoparticles are considered single ferromagnetic domains, in which all spins are strongly coupled. Due to the small size of the particles, the magnetic energy of the particles is of the order of the thermal energy, therefore, the direction of the total magnetic moment of the single magnetic particles fluctuates significantly from equilibrium positions resulting in superparamagnetic behavior [39]. At lower temperatures, however, some superparamagnetic particles are blocked revealing ferrimagnetic behavior as expected for magnetite nanoparticles. The highest blocking temperature (T_B = 290 K) was found for the uncoated magnetite nanoparticles (Fig. 8C), while it was 190 K and 105 K for the coated samples Co-MION-CMC (Fig. 8B) and MION-CMC (Fig. 8A), respectively. For sample MION-CMC_07_90 (Fig. 9A), the magnetic hysteresis was still small at 77 K, indicating nanoparticles which are magnetically soft. Conversely, the Co-doping of MION sample caused magnetically harder nanoparticles when compared to MION-CMC, which is revealed by the stronger hysteresis and higher coercivity field at 77 K (Fig. 9B), in agreement with the results obtained by magnetic resonance.

In addition to the magnetic properties for comparison and reference purposes, the morphological and physicochemical characterizations of uncoated Fe_3O_4 nanoparticles (without CMC ligand) were also evaluated and presented in *Supplementary Material* (Fig. 9S).

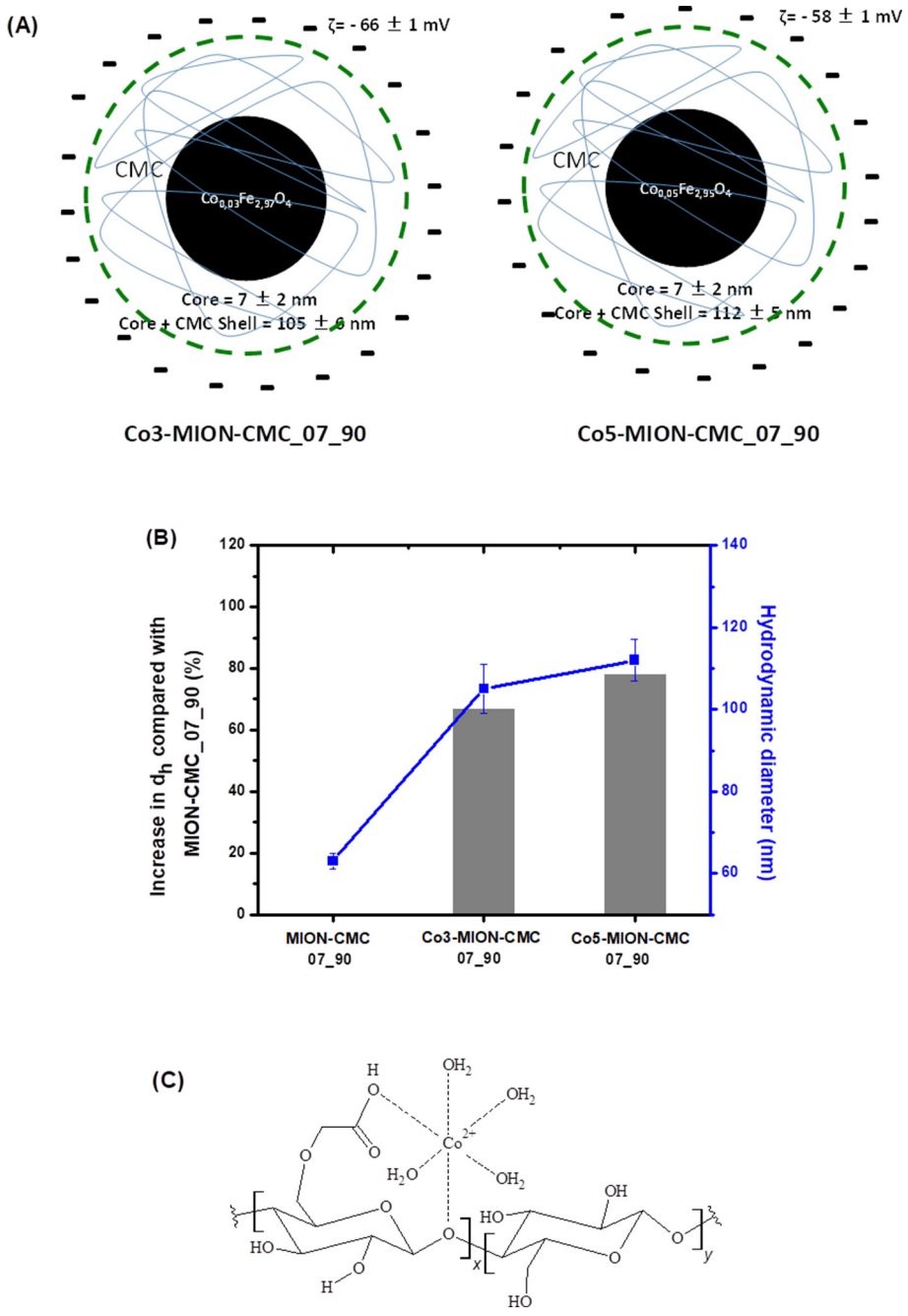

Fig. 6. (A) Schematic representation of core-shell structures of nanoconjugates Co3-MION-CMC_07_90 and Co5-MION-CMC_07_90 (pH = 7.0 ± 0.5). (B) Effect of Co-doping on the relative increase (%) of d_h of nanoconjugates compared to Fe_3O_4-CMC. (C) Suggested schematic representation for the formation of coordination complexes between Co^{2+} and COO^-/CMC (not to scale).

3.4. Biological characterization of MION

3.4.1. Cell viability in vitro – mitochondrial activity (MTT) assay

MTT cell viability test (3-(4,5-dimethylthiazol-2yl-) 2,5-diphenyl tetrazolium bromide) has been considered the major assay for *in vitro* assessment of cytotoxicity of bio(nano)materials for biomedical applications. Therefore, MTT bioassay was performed to evaluate the potential *in vitro* cell viability responses of nanoconjugates towards normal (HEK 293 T) and human cancer cell lines (U87, glioblastoma). The results of MTT for normal (HEK 293 T, Fig. 10A) and cancer (U87, Fig. 10B) cells incubated with Fe_3O_4-CMC nanocolloids (CMC, DS = 0.7 and M_w = 90 kDa) demonstrated no cytotoxicity at lower concentrations of 0.8 and 1.7 μg.mL^{-1}, where the average cell viability responses were typically over 80% for both cell types. Therefore, according to the literature and based on the international standard (ISO 10933-5 - Biological evaluation of medical devices - Part 5: Tests for *in vitro* cytotoxicity), (nano)materials with cell viability results higher than 70% are considered non-cytotoxic (*in vitro*) and preliminarily appropriate for biomedical applications. However, at higher concentrations of iron oxide nanoparticles (*e.g.*, 4.2, 8.5, and 17.0 μg/mL), it was observed moderate cytotoxicity by the reduction of cell viability responses (*i.e.*, cell viability < 70%), which indicated the dependence of cytotoxicity effect with the concentration of nanoconjugates. Certainly, at much higher concentrations, it is conceivable to expect that most (nano)materials are likely to present unneglectable levels of toxicity to cells, as they can interfere and cause disruption to the cellular

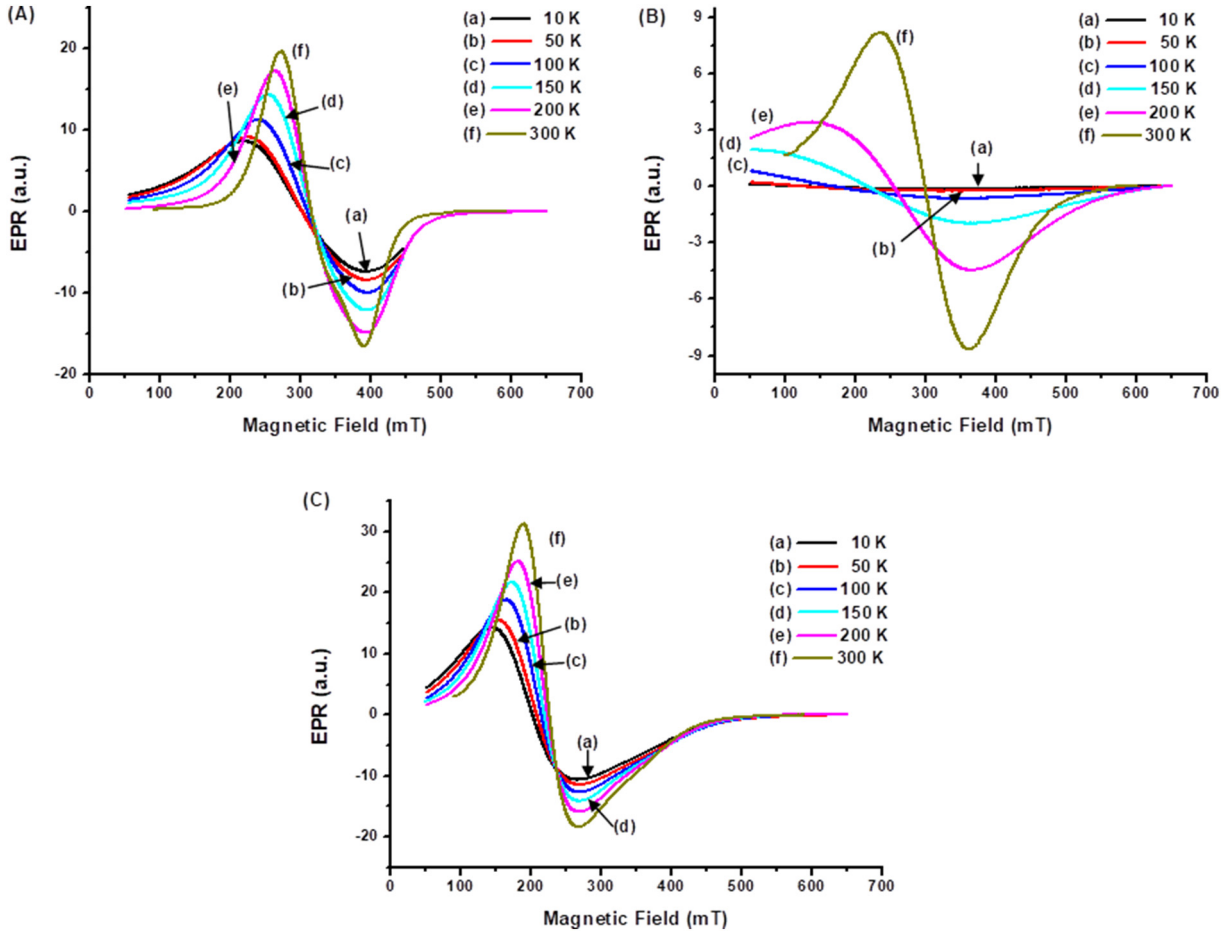

Fig. 7. EPR spectra of (A) MION-CMC_07_90, (B) Co5-MION-CMC_07_90 and (C) uncoated magnetite as a function of temperature (T).

metabolism, which has been reported in the literature for iron oxide nanoparticles [7]. In addition, the cell viability tests indicated similar trends with slightly different responses for CMC polymers with the higher degree of carboxymethylation and molar mass (DS = 1.2, M_w = 250 kDa) used for the synthesis of iron oxide nanoparticles, but the results (Fig. 10S, *Supplementary Material*) were statistically equivalent (Bonferroni Multiple Analysis Test, one-way analysis of variance, α = 0.05). These results suggest that the higher concentration of negative charges (-COO^-) of CMC (DS = 1.2) of the nanoconjugates may have altered the electrostatic interactions at the cell-nanoconjugates interfaces, but not sufficiently for affecting the cytotoxicity response towards these nanoconjugates. It is important to mention that these findings can be significantly modified by using different size/size distribution, shape, surface coating, chemical composition and others aspects of the nanoparticles, considering that their physicochemical properties are essential to determine the cytotoxicity [40,41]. For that reason, it is of paramount importance to comprehensively characterize the morphological and structural properties of nanoparticulate systems before performing biological tests related to their cytotoxicity or cell killing activity as the results are strongly dependent on the overall contributions from the core and shell entities.

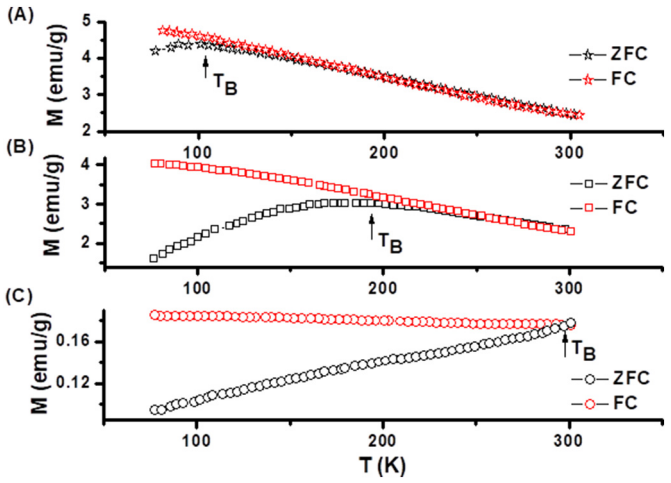

Fig. 8. Magnetization curves of samples (A) MION-CMC_07_90, (B) Co5-MION-CMC_07_90 and (C) uncoated magnetite in the temperature range from 300 K to 77 K, for zero-field cooling (ZFC) and after applying a field of 70 Oe for field cooling (FC).

3.5. Magnetic hyperthermia of nanocolloids

3.5.1. Magnetic hyperthermia test in vitro acellular

The iron oxide nanoconjugates were exposed to an alternating magnetic field (AMF) of 19.9 kA/m for 30 min in order to investigate the thermal effects, referred to as magnetic hyperthermia analysis (MT). The samples were placed inside a polystyrene tube in order to prevent the occurrence of non-specific heating. Considering the Fe_3O_4 nanoparticles stabilized by different CMC polymers, it was observed (Fig. 11A) that the MION-CMC_07_90 sample showed higher heating rate compared to other nanoconjugates when exposed to the magnetic field. The hyperthermia response was reduced by the presence of the CMC polymer coating onto the iron nanoparticles needed for the stabilization as colloids in aqueous medium because of the relative decrease of mass of magnetic material (*i.e.*, iron oxide component) per volume of nanoparticle (*i.e.*, hydrodynamic volume, d_h) [42]. Considering the results

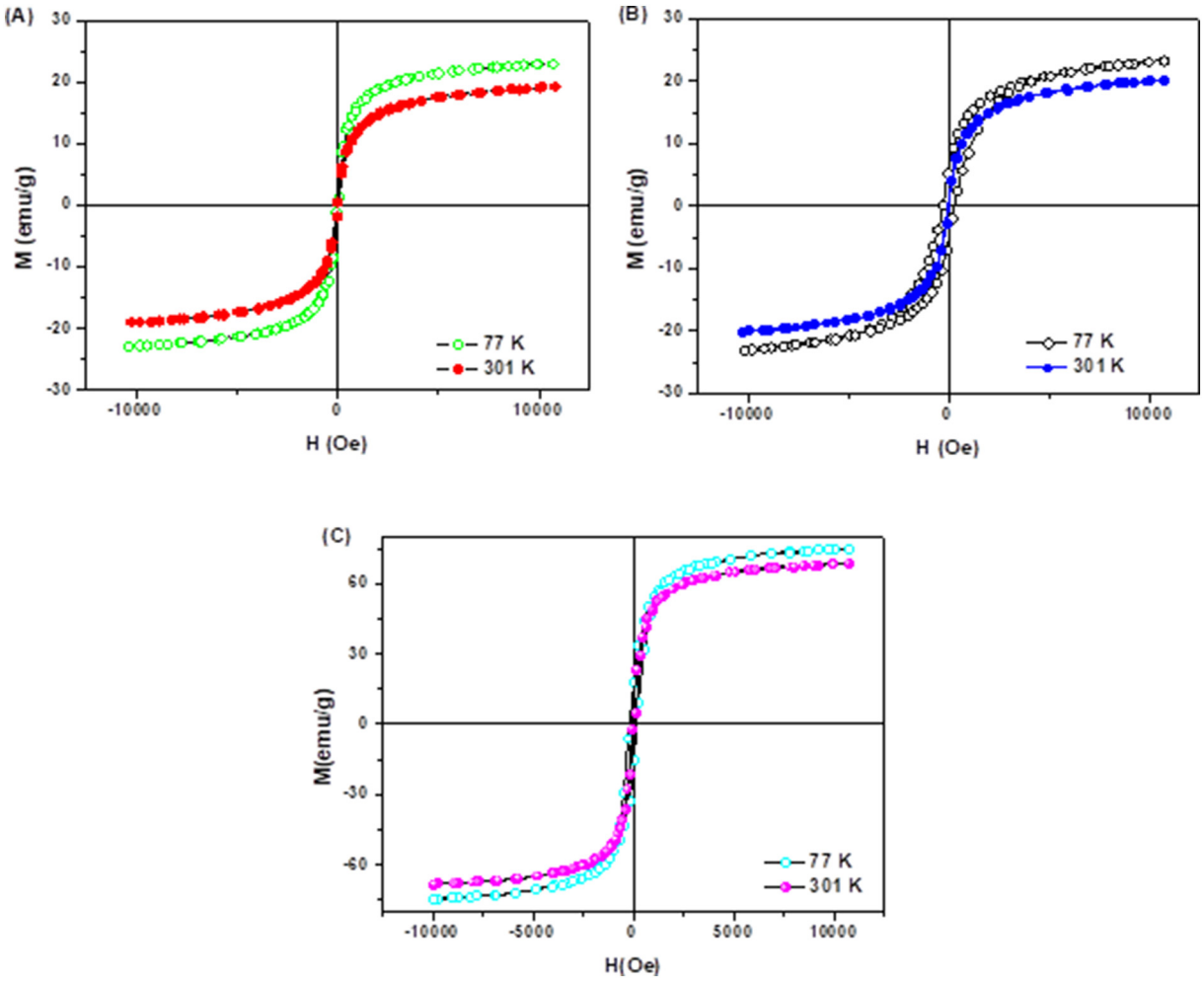

Fig. 9. Hysteresis curves for samples (A) MION-CMC_07_90, (B) Co5-MION-CMC_07_90 and (C) uncoated magnetite measured at 77 K and 300 K as a function of the magnetic field −10,000 Oe < H < 10,000 Oe.

of Section 3.2, where the MION-CMC_07_250 and MION-CMC_12_250 samples presented the larger d_h values, it was calculated lower values for the ratio based on the "mass of magnetic nanomaterial" per volume of nanocolloids, which was accounted for the reduction of magnetic hyperthermia responses. In this study, it is suggested for the first time the parameter based on the ratio [D_{core}/d_h] for assessing the combined effects of nanocolloidal ferrofluids composed by the inorganic core (iron oxide) and the organic shell (CMC, polymer) under alternating magnetic field. Thus, the decrease of D_{core}/d_h ratio as the hydrodynamic volume increase (Fig. 11A) evidenced the relative reduction of "magnetic

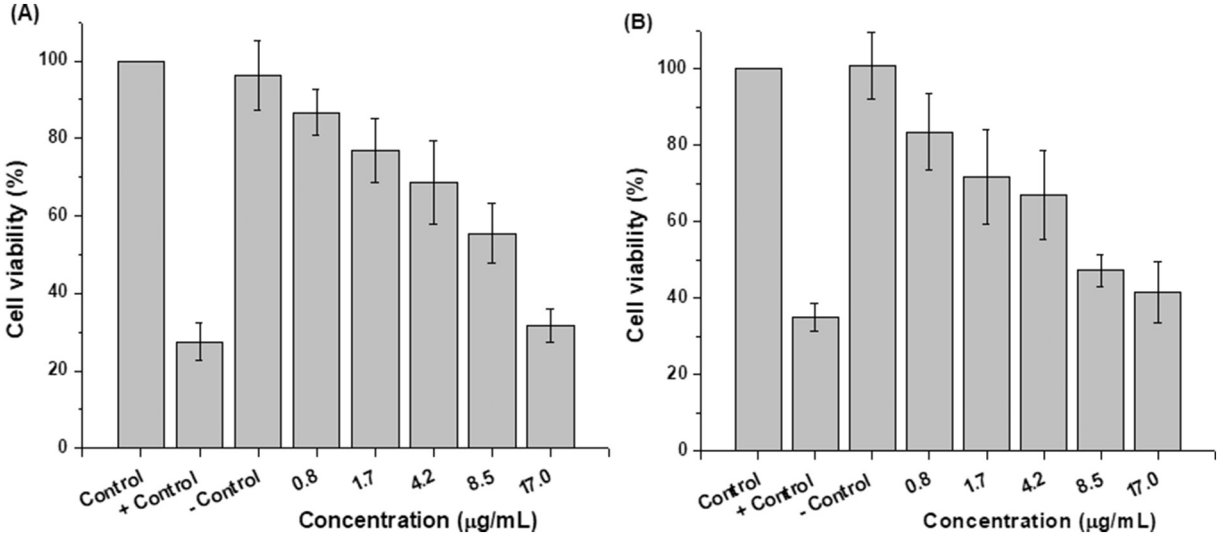

Fig. 10. MTT *in vitro* assays for normal (HEK 293 T, (A)) and cancer (U87, (B)) cells incubated with MION-CMC nanocolloids (CMC, DS = 0.7 and M_w = 90 kDa).

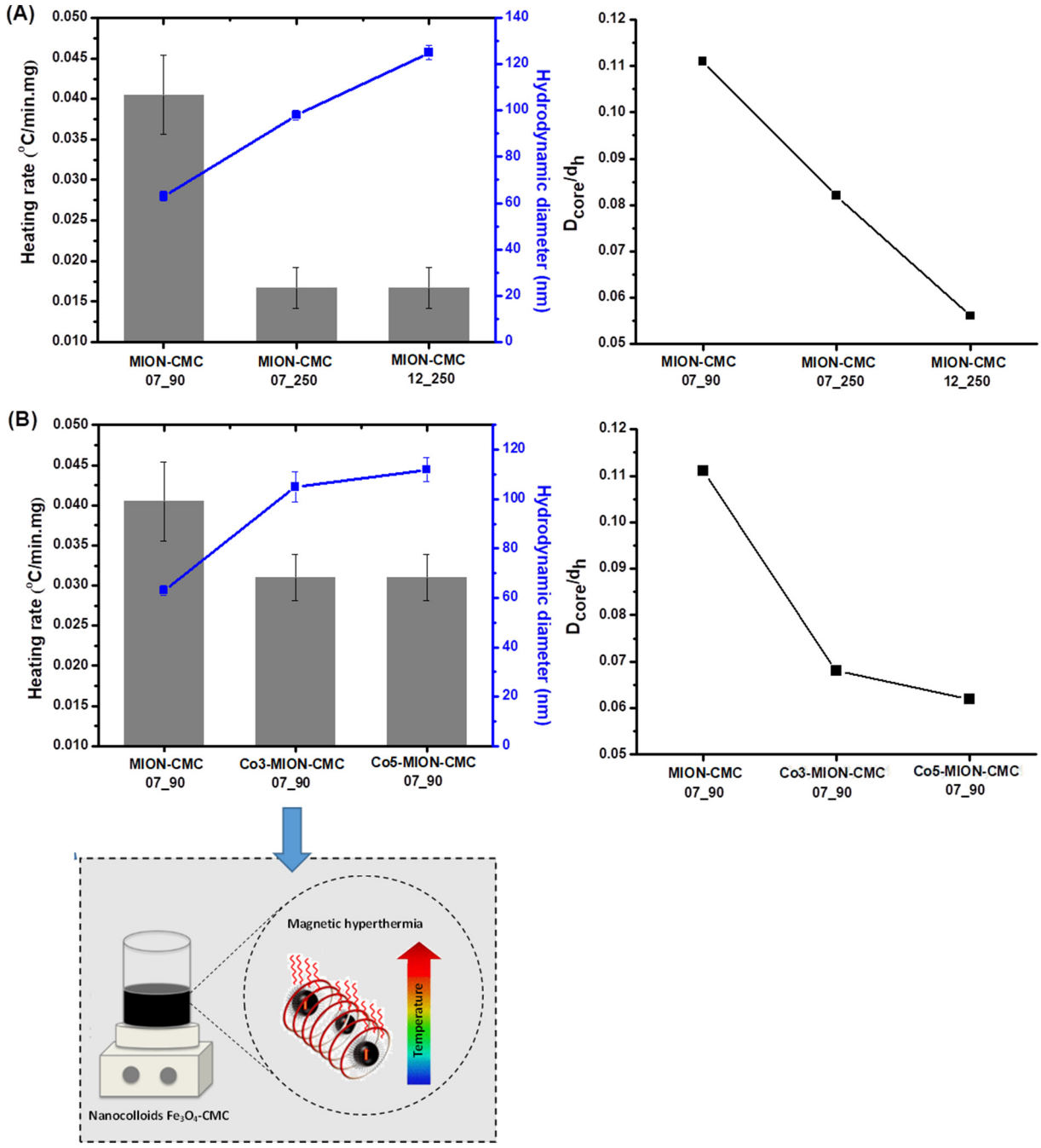

Fig. 11. Heating rate and d_h values and D_{core}/d_h ratio showing (A) Effect of M_w and DS of CMC and (B) Effect of Co-doping.

response" of the nanocolloids, which is only generated by the core nanomaterial. These assumptions are endorsed by the results discussed in Section 3.2 where nanocrystalline structures, core sizes and ZP values were similar for these samples, but with distinct values of d_h. Moreover, it was observed that the cobalt-doped nanoparticles (Co-MIONs) presented lower heating rates compared to undoped Fe_3O_4 nanoparticles (MIONs) submitted to the alternating magnetic field for hyperthermia test (Fig. 11B). This behavior was also assigned to the relative colloidal volume (d_h) of nanoconjugates because the Co-MION-CMC nanoconjugates showed higher values, leading to lower thermal response under magnetic hyperthermia. Based on the literature [43], the partial replacement of Fe^{2+} by Co^{2+} species in magnetite nanoparticles is a useful strategy to improve hyperthermia properties, because Co^{2+} usually increases the magnetic anisotropy of the system. However, this trend was not observed in this study probably because the incorporation of Co^{2+} in the iron oxides enlarged the hydrodynamic volume overcoming the effect on the anisotropy of the system. According to the literature [44], the mechanisms responsible for heat generation of iron oxide magnetic nanoparticles are very complex and not entirely understood yet, which are size dependent and influenced by relaxation processes. It should be highlighted that higher heating rate is not necessarily positive for biomedical applications because elevated temperatures generated by magnetic hyperthermia can kill cancer cells but also harm adjacent cells and tissues.

3.5.2. Hyperthermia test in vitro with brain cancer cells

In order to preliminary assessing the potential applications of the nanoconjugates in killing cancer cells, magnetic hyperthermia analyses

were performed as a proof of concept with human brain cancer cells (glioma cells, U87). The iron oxide nanoconjugates (MION-CMC_07_90) were selected for this *in vitro* assay with tumor cells based on the results of higher MT heating rate in the previous section. In Fig. 12 is presented the cell viability responses of brain cancer cells after incubation with MION-CMC_07_90 nanoconjugates for 3 h submitted to the *in vitro* magnetotherapy assay (MT). As reference (U87-MION-CMC), it was observed that the cell viability was reduced to approximately 60% after incubation with magnetite nanoparticles without MT, which evidenced intrinsic cytotoxic effect of these nanoparticles.

More importantly, the cell viability response was remarkably reduced to 34% when the glioma cancer cells were incubated with the Fe_3O_4-CMC nanocolloids and exposed to the alternating magnetic field (U87-MION-CMC-MT). This significant reduction of cell viability after magnetic hyperthermia process proved the hypothesis that these novel nanocolloids composed of Fe_3O_4 core and CMC shell behaved as nanoheaters when submitted to alternating magnetic field (AMF). This localized heat generated by the nanoconjugates under AMF increases the temperature by 5–6 °C, which can induce cellular necrosis and/or apoptosis (cell death showed in Fig. 11S, *Supplementary Material*) usually referred to as magnetotherapy of cancer [7]. Finally, it should be stressed that the magnetic hyperthermia assay for killing brain cancer cells *in vitro* using this novel magnetite-CMC nanoconjugates was presented as a proof of concept for potential applications as an additional supporting therapy for cancer treatment. To this end, other chemical compositions for altering the inorganic core of the nanoparticle and other polymer ligands for changing the organic shell can significantly modify the killing activity of the iron oxide nanohybrids produced *via* aqueous colloidal process. As mentioned before, normal cells (HEK 293T) were not submitted to MT assay because CMC does not provide the required selectivity and specificity for killing cancer cells while preserving normal ones. That could be achieved by biofunctionalization of CMC with specific molecules (folic acid, peptides, antibodies, *etc.*) for targeting cancer cells, but this approach is beyond the scope of this study. Therefore, further studies are certainly needed in the future for investigating other relevant aspects before performing *in vivo* assays and clinical trials for treating brain tumors, which is highly challenging and beyond the scope of the present research. Nonetheless, this study offers novel nanofluids with promising future perspectives for developing magnetic guided surgery and magnetic hyperthermia to be applied in the treatment of cancer tumors.

4. Conclusions

The results proved that Fe_3O_4 and $Co_xFe_{3-x}O_4$ nanoparticles (MION and Co-MION, respectively) were produced in a single-step one-pot process in aqueous media using CMC with different DS and molar mass. The efficient stabilization of these nanocolloids in aqueous media was attributed to the interactions of functional groups of CMC with the surfaces of the nanoparticles leading to the formation of core-shell nanostructures. The results demonstrated that the MION-CMC and Co-MION-CMC nanoparticles were produced with fairly monodispersed (average size = 7 nm) and spherical morphology. The cobalt-doping decreased the average size of the iron oxide nanocrystals and affected the d_h of the nanocolloids, which was attributed to the interactions between the Co^{2+} at the surface of the nanoparticles with CMC carboxylates functional groups. Moreover, the functionalization of CMC with higher concentration of carboxylates groups caused a drastic increase of approximately 100% on the d_h (*i.e.*, DS = 0.7 compared to DS = 1.2), which was attributed to the volume of solvation layer of water molecules to balance the negatively charged groups of the nanocolloids. EPR spectroscopy and *VSM* results endorsed the formation of magnetic particles with superparamagnetic behavior due to the nanosize dimensions. Based on the MTT assay considering the international standard (ISO 10933-5), the cell viability results were dependent on the concentration of the magnetite nanoparticles, varying from non-toxic response at lower concentrations (<[4.2 g mL^{-1}]) to moderate cytotoxicity at higher concentrations (>[4.2 g mL^{-1}]) for both cell types. Moreover, the magnetic hyperthermia analyses demonstrated the influence of the CMC characteristics (DS and M_w) and cobalt-doping of nanocolloids on the generated heat, which was assigned to changes of the magnetic relaxation phenomena on the core-shell nanostructures. Additionally, the hyperthermia results proved the remarkable killing activity against brain cancer cells *in vitro* (U87 cells) after the incubation with MION-CMC and applying alternating magnetic field. Therefore, these new iron oxide-CMC magnetic nanocolloids can offer promising future perspectives as localized *nanoheaters* for magnetic hyperthermia therapy associated with other treatments of cancer therapy.

Funding sources

This work was supported by the following Brazilian research agencies: CAPES (PROEX- 433/2010; PNPD; PROINFRA2010–2014);

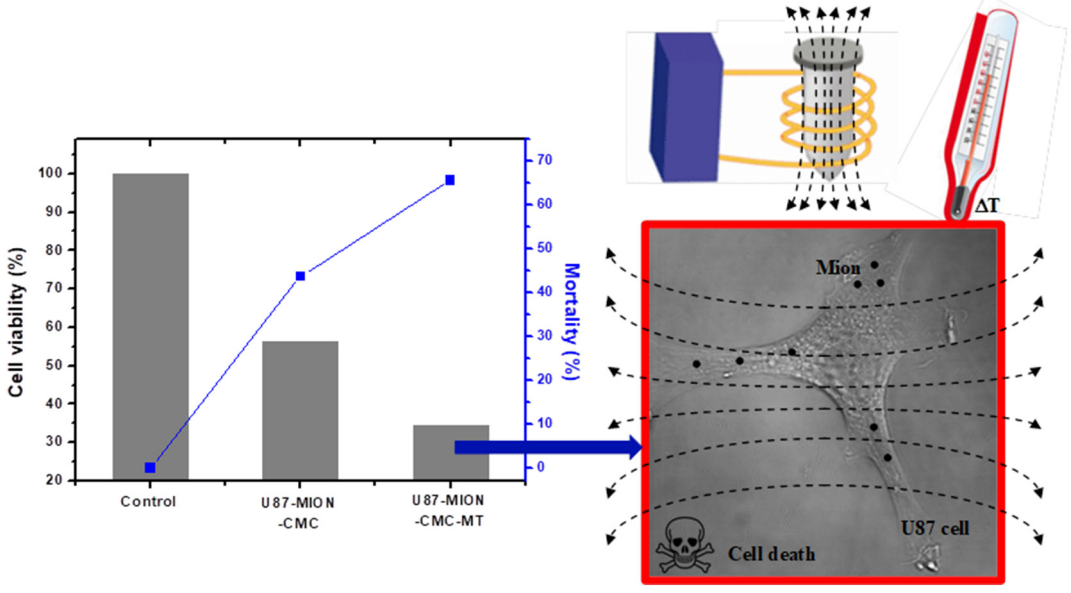

Fig. 12. Cell viability response (left) of the U87 cells incubated with MION-CMC_07_90 system in the absence (U87-MION-CMC) and presence of alternating magnetic field (U87-MION-CMC-MT). Schematic representation of the magnetic hyperthermia process on U87 with Fe_3O_4-CMC conjugates (right, not to scale).

FAPEMIG (PPM- 00760-16; BCN-TEC 30030/12; UNIVERSAL-APQ-00291-18); CNPq (PQ1B-306,306/2014-0; PQ1A-303,893/2018-4; UNIVERSAL-457537/2014-0; 421312/2018-1; PIBIC-2014/2015); and FINEP (CTINFRA-PROINFRA 2008/2010/2011).

Conflicts of interest

The authors declare that they have no competing interests.

Acknowledgments

The authors thank the staff at the Center of Nanoscience, Nanotechnology and Innovation (CeNano^{2}I)/CEMUCASI/UFMG and the Center of Microscopy/UFMG for the characterization facilities.

Appendix A. Supplementary data

Supplementary data to this article can be found online at https://doi.org/10.1016/j.ijbiomac.2019.04.006.

References

[1] N.S.V. Capanema, A.A.P. Mansur, A.C. Jesus, S.M. Carvalho, L.C. Oliveira, H.S. Mansur, Superabsorbent crosslinked carboxymethylcellulose - PEG hydrogels for potential wound dressing applications, Int. J. Biol. Macromol. 106 (2018) 1218–1234, https://doi.org/10.1016/j.ijbiomac.2017.08.124.

[2] H. Chen, W. Zhang, G. Zhu, J. Xie, X. Chen, Rethinking cancer nanotheranostics, Nat. Rev. Mater. 2 (2017) 1–18, https://doi.org/10.1038/natrevmats.2017.24.

[3] J. Li, Y. Li, Y. Wang, W. Ke, W. Chen, W. Wang, Z. Ge, Polymer prodrug-based nanoreactors activated by tumor acidity for orchestrated oxidation/chemotherapy, Nano Lett. 17 (2017) 6983–6990, https://doi.org/10.1021/acs.nanolett.7b03531.

[4] A.A.P. Mansur, S.M. Carvalho, Z.I.P. Lobato, M.F. Leite, A.S. Cunha, H.S. Mansur, Design and development of polysaccharide-doxorubicin-peptide bioconjugates for dual synergistic effects of integrin-targeted and cell-penetrating peptides for cancer chemotherapy, Bioconjug. Chem. 29 (2018) 1973–2000, https://doi.org/10.1021/acs.bioconjchem.8b00208.

[5] J. Shi, P.W. Kantoff, R. Wooster, O.C. Farokhzad, Cancer nanomedicine: progress, challenges and opportunities, Nat. Rev. Cancer 17 (2017) 20–37, https://doi.org/10.1038/nrc.2016.108.

[6] Y. Yang, A. Roy, Y. Zhao, E. Undzys, S.D. Li, Comparison of tumor penetration of podophyllotoxin-carboxymethylcellulose conjugates with various chemical compositions in tumor spheroid culture and in vivo solid tumor, Bioconjug. Chem. 28 (2017) 1505–1518, https://doi.org/10.1021/acs.bioconjchem.7b00165.

[7] S. Balasubramanian, R.G. Aswathy, Y. Nagaoka, M. Suzuki, T. Fukuda, Y. Yoshida, T. Maekawa, D.N. Sakthikumar, Multifunctional carboxymethyl cellulose - based magnetic nanovector as a theranostic system for folate receptor targeted chemotherapy, imaging, and hyperthermia against cancer, Langmuir 29 (2013) 3453–3466, https://doi.org/10.1021/la305048m.

[8] X. Guo, L. Xue, W. Lv, Q. Liu, R. Li, Z. Li, J. Wang, Facile synthesis of magnetic carboxymethylcellulose nanocarriers for pH-responsive delivery of doxorubicin, New J. Chem. 39 (2015) 7340–7347, https://doi.org/10.1039/C5NJ01190F.

[9] M. Saeed, W. Ren, A. Wu, Therapeutic applications of iron oxide based nanoparticles in cancer: basic concepts and recent advances, Biomater. Sci. 6 (2018) 708–725, https://doi.org/10.1039/C7BM00999B.

[10] K. Venkatesan, D.R. Babu, M. Bai, R. Supriya, R. Vidya, S. Madeswaran, P. Anandan, M. Arivanandhan, Y. Hayakawa, Structural and magnetic properties of cobalt-doped iron oxide nanoparticles prepared by solution combustion method for biomedical applications, Int. J. Nanomed. 10 (2015) 189–198, https://doi.org/10.2147/IJN.S82210.

[11] A. López-Ortega, E. Lottini, G. Bertoni, C.J. Fernández, C. Sangregorio, Topotaxial phase transformation in cobalt doped iron oxide core/shell hard magnetic nanoparticles, Chem. Mater. 29 (2017) 1279–1289, https://doi.org/10.1021/acs.chemmater.6b04768.

[12] Z. Chen, D. Wei, Q. Li, X. Wang, S. Yu, L. Liu, B. Liu, S. Xiu, J. Wang, D. Chen, T. Hayat, X. Wang, Macroscopic and microscopic investigation of Cr(VI) immobilization by nanoscaled zero-valent iron supported zeolite MCM-41 via batch, visual, XPS and EXAFS techniques, J. Clean. Prod. 181 (2018) 745–752, https://doi.org/10.1016/j.jclepro.2018.01.231.

[13] P. Xiu, G.M. Zeng, D.L. Huang, C.L. Feng, S. Hu, M.H. Zhao, C. Lai, Z. Wei, C. Huang, G.X. Xie, Z.F. Liu, Use of iron oxide nanomaterials in wastewater treatment: a review, Sci. Total Environ. 424 (2012) 1–10, https://doi.org/10.1016/j.scitotenv.2012.02.023.

[14] C. Azevedo, M.H. Macedo, B. Sarmento, Strategies for enhanced intracellular delivery of nanomaterials, Drug Discov. Today 23 (2018) 944–959, https://doi.org/10.1016/j.drudis.2017.08.011.

[15] S.M. Carvalho, H.S. Mansur, F.P. Ramanery, A.A.P. Mansur, Z.I.P. Lobato, M.F. Leite, Cytotoxicity investigation of luminescent nanohybrids based on chitosan and carboxymethyl chitosan conjugated with Bi_2S_3 quantum dots for biomedical applications, Toxicol. Res. 5 (2016) 1017–1028, https://doi.org/10.1039/C6TX00039H.

[16] V. Mameli, A. Musinu, A. Ardu, G. Ennas, D. Peddis, D. Niznansky, C. Sangregorio, C. Innocenti, N.T. Thanh, C. Cannas, Studying the effect of Zn-substitution on the magnetic and hyperthermic properties of cobalt ferrite nanoparticles, Nanoscale 8 (2016) 10124–10137, https://doi.org/10.1039/c6nr01303a.

[17] N. Habibi, Preparation of biocompatible magnetite-carboxymethyl cellulose nanocomposite: characterization of nanocomposite by FTIR, XRD, FEEM and TEM, Spectrochim. Acta A 131 (2014) 55–58, https://doi.org/10.1016/j.saa.2014.04.039.

[18] J.F. Su, Z. Huang, X.Y. Yuan, X.Y. Wang, M. Li, Structure and properties of carboxymethyl cellulose/soy protein isolate blend edible films crosslinked by maillard reactions, Carbohydr. Polym. 79 (2010) 145–153, https://doi.org/10.1016/j.carbpol.2009.07.035.

[19] G. Kandasamy, A. Sudame, T. Luthra, K. Saini, D. Maity, Functionalized hydrophilic superparamagnetic iron oxide nanoparticles for magnetic fluid hyperthermia application in liver cancer treatment, ACS Omega 3 (2018) 3991–4005, https://doi.org/10.1021/acsomega.8b00207.

[20] S. Sheikholeslami, G.D. Domiri, J.M. Younus, R. Ellahi, Effect of thermal radiation on magnetohydrodynamics nanofluids flow and heat transfer by means of two phase model, J. Magn. Magn. Mater. 374 (2015) 125–138, https://doi.org/10.1016/j.jmmm.2014.08.021.

[21] D.G. Silva, S.H. Toma, F.M. Melo, L.V.C. Carvalho, A. Magalhães, E. Sabadini, A.D. Santos, K. Araki, H.E. Toma, Direct synthesis of magnetite nanoparticles from iron (II) carboxymethylcellulose and their performance as NMR contrast agents, J. Magn. Magn. Mater. 397 (2016) 28–32, https://doi.org/10.1016/j.jmmm.2015.08.092.

[22] M. Zirak, A. Abdollahiyan, B. Eftekhari-Sis, M. Saraei, Carboxymethyl cellulose coated Fe_3O_4@SiO_2 core–shell magnetic nanoparticles for methylene blue removal: equilibrium, kinetic, and thermodynamic studies, Cellulose 25 (2018) 503–515, https://doi.org/10.1007/s10570-017-1590-5.

[23] N.S.V. Capanema, A.A.P. Mansur, S.M. Carvalho, I.C. Carvalho, P. Chagas, L.C.A. De Oliveira, H.S. Mansur, Bioengineered carboxymethyl cellulose-doxorubicin prodrug hydrogels for topical chemotherapy of melanoma skin cancer, Carbohydr. Polym. 195 (2018) 401–412, https://doi.org/10.1016/j.carbpol.2018.04.105.

[24] S. Anjum, R. Tufail, K. Rashid, R. Zia, S. Riaz, Effect of cobalt doping on crystallinity, stability, magnetic and optical properties of magnetic iron oxide nanoparticles, J. Magn. Magn. Mater. 425 (2017) 198–207, https://doi.org/10.1016/j.jmmm.2017.02.006.

[25] B. Babukutty, S.S. Nair, N. Kalarikkal, Studies on structural, optical and magnetic properties of cobalt substituted magnetite fluids ($Co_xFe_{1-x}Fe_2O_4$), Mater. Res. Express 4 (2017) 1–46, https://doi.org/10.1088/2053-1591/aa628b.

[26] C.N. Zwicky, P. Lienemann, Quantitative or semi-quantitative? – laboratory-based WD-XRF versus portable ED-XRF spectrometer: results obtained from measurements on nickel-base alloys, X-Ray Spectrom. 33 (2004) 294–300, https://doi.org/10.1002/xrs.730.

[27] A.A.P. Mansur, F.G. Carvalho, R.L. Mansur, S.M. Carvalho, L.C. Oliveira, H.S. Mansur, Carboxymethylcellulose/ZnCdS fluorescent quantum dot nanoconjugates for cancer cell bioimaging, Int. J. Biol. Macromol. 96 (2017) 675–686, https://doi.org/10.1016/j.ijbiomac.2016.12.078.

[28] C.L. Lin, C.F. Lee, W.Y. Chiu, Preparation and properties of poly (acrylic acid) oligomer stabilized superparamagnetic ferrofluid, J. Colloid Interface Sci. 291 (2005) 411–420, https://doi.org/10.1016/j.jcis.2005.05.023.

[29] V.S. Kumbhar, A.D. Jagadale, N.M. Shinde, C.D. Lokhande, Chemical synthesis of spinel cobalt ferrite ($CoFe_2O_4$) nano-flakes for supercapacitor application, Appl. Surf. Sci. 259 (2012) 39–43, https://doi.org/10.1016/j.apsusc.2012.06.034.

[30] B.J. Rani, M. Ravina, B. Saravanakumar, G. Ravi, V. Ganesh, S. Ravichandran, Ferrimagnetism in cobalt ferrite ($CoFe_2O_4$) nanoparticles, Nano-Struct. Nano-Objects 14 (2018) 84–91, https://doi.org/10.1016/j.nanoso.2018.01.012.

[31] G.V.M. Jacintho, A.G. Brolo, P. Corio, P.A.Z. Suarez, J.C. Rubim, Structural investigation of MFe_2O_4 (M = Fe, Co) magnetic fluids, J. Phys. Chem. C 133 (2009) 7684–7691, https://doi.org/10.1021/jp9013477.

[32] A.A.P. Mansur, H.S. Mansur, R.L. Mansur, F.G. Carvalho, S.M. Carvalho, Bioengineered II-IV semiconductor quantum dot-carboxymethylcellulose nanoconjugates as multifunctional fluorescent nanoprobes for bioimaging live cells, Spectrochim. Acta A 189 (2018) 393–404, https://doi.org/10.1016/j.saa.2017.08.049.

[33] A.H. Basta, H. El-Saied, Characterization of polymer complexes by thermal and IR spectral analyses, Polym.-Plast. Technol. Eng. 39 (2000) 887–904, https://doi.org/10.1081/PPT-100101411.

[34] A.J. Ward, A.F. Masters, T. Maschmeyer, Cobalt(II) carboxylate chemistry and catalytic applications, in: J. Reedijk, L. Casella, K. Poeppelmeier (Eds.),Comprehensive Inorganic Chemistry II, Sydney 2013, pp. 665–684.

[35] N. Noginova, F. Chen, T. Weaver, E.P. Giannelis, A.B. Bourlinos, V.A. Atsarkin, Magnetic resonance in nanoparticles: between ferro- and paramagnetism, J. Phys. Condens. Matter 19 (2007) 1–15, https://doi.org/10.1088/0953-8984/19/24/246208.

[36] Y.A. Koksharov, D.A. Pankratov, S.P. Gubin, I.D. Kosobudsky, M. Beltran, Y. Khodorkovsky, A.M. Tishin, Electron paramagnetic resonance of ferrite nanoparticles, J. Appl. Physiol. 89 (2001) 2293–2298, https://doi.org/10.1063/1.1332417.

[37] J. Kliava, R. Berger, Size and shape distribution of magnetic nanoparticles in disordered systems: computer simulations of superparamagnetic resonance spectra, J. Magn. Magn. Mater. 205 (1999) 328–342, https://doi.org/10.1016/S0304-8853(99)00510-7.

[38] N. Bao, L. Shen, Y. Wang, P. Padhan, A. Gupta, A facile thermolysis route to monodisperse ferrite nanocrystals, J. Am. Chem. Soc. 129 (2007) 12374–12375, https://doi.org/10.1021/ja074458d.

[39] E. de Biasi, C.A. Ramos, R.D. Zysler, Size and anisotropy determination by ferromagnetic resonance in dispersed magnetic nanoparticle systems, J. Magn. Magn. Mater. 262 (2003) 235–241, https://doi.org/10.1016/S0304-8853(02)01496-8.

[40] J. Hou, Y. Zhou, C. Wang, S. Li, X. Wang, Toxic effects and molecular mechanism of different types of silver nanoparticles to the aquatic crustacean *Daphnia magna*, Environ. Sci. Technol. 51 (2017) 12868–12878, https://doi.org/10.1021/acs.est.7b03918.
[41] J. Hou, H. Liu, L. Wang, L. Duan, S. Li, X. Wang, Molecular toxicity of metal oxide nanoparticles in *Danio rerio*, Environ. Sci. Technol. 52 (2018) 7996–8004, https://doi.org/10.1021/acs.est.8b01464.
[42] G. Iglesias, A.V. Delgado, M. Kujda, M.M. Ramos-Tejada, Magnetic hyperthermia with magnetite nanoparticles: electrostatic and polymeric stabilization, Colloid Polym. Sci. 249 (2016) 1541–1550, https://doi.org/10.1007/s00396-016-3918-3.
[43] E. Fantechi, C. Innocenti, M. Albino, E. Lottini, Influence of cobalt doping on the hyperthermia efficiency of magnetite nanoparticles, J. Magn. Magn. Mater. 380 (2015) 365–371, https://doi.org/10.1016/j.jmmm.2014.10.082.
[44] S. Tong, C.A. Quinto, L. Zhang, P. Mohindra, G. Bao, Size-dependent heating of magnetic iron oxide nanoparticles, ACS Nano 11 (2017) 6808–6816, https://doi.org/10.1021/acsnano.7b01762.